Catalysis Science & Technology

Accepted Manuscript

ROYAL SOCIETY OF CHEMISTRY

www.rsc.org/catalysis

Graphical abstract

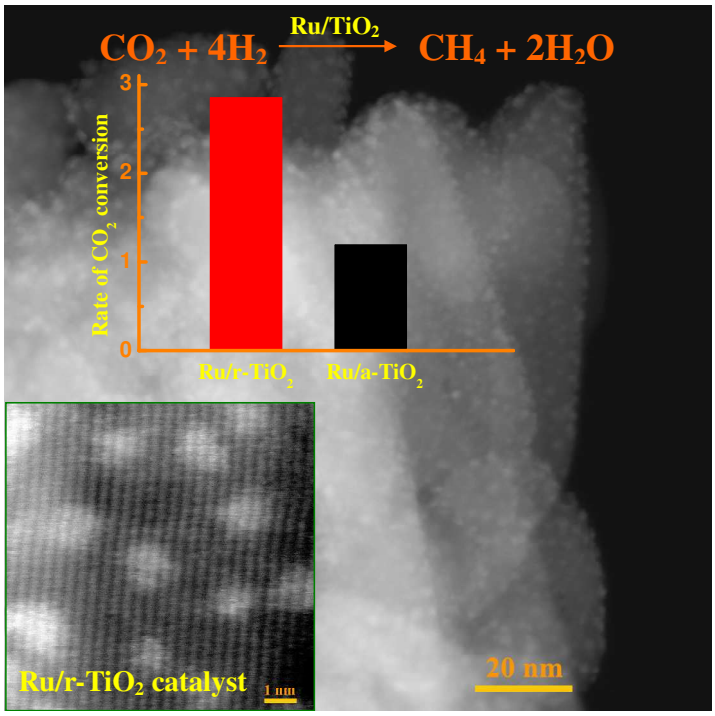

Rutile-type TiO_2 is a promising support for preparing a highly dispersed Ru catalyst, which exhibited high activity in CO_2 methanation.

Catalysis
Science & Technology

Cite this: DOI: 10.1039/c0xx00000x

PAPER

www.rsc.org/xxxxxx

Crystal Phase Effects on the Structure and Performance of Ruthenium Nanoparticles for the CO_2 Hydrogenation

Qingquan Lin,[a,b,c] Xiao Yan Liu,[a] Ying Jiang,[d] Yong Wang,[d] Yanqiang Huang,*[a] and Tao Zhang[a]

Received (in XXX, XXX) Xth XXXXXXXXX 20XX, Accepted Xth XXXXXXXXX 20XX
DOI: 10.1039/b000000x

The effect of TiO_2 phase structure on the dispersion of Ru nanoparticles was investigated in this study. Rutile-type TiO_2 (r-TiO_2) appears to be a superior support to prohibit the aggregation of RuO_2 during the calcination in air. Compared with anatase-type TiO_2 (a-TiO_2) supported Ru nanoparticles (4.0 ± 2.4 nm), r-TiO_2 supported ones exhibited a quite narrower particle size distribution (1.1 ± 0.2 nm). This unique property was contributed to a strong interaction between RuO_2 and r-TiO_2 in terms of the formation of Ru-O-Ti bond, which was confirmed by the X-ray absorption measurements and H_2-TPR experiments. To great extent, this strong interaction not only promotes Ru nanoparticles highly dispersed, but also prevents their aggregation. As a result, the Ru/r-TiO_2 catalysts displayed a much higher activity and thermal stability than the Ru/a-TiO_2 in the reaction of CO_2 methanation.

1. Introduction

Supported metal nanoparticles are widely used in a great variety of catalytic applications. The activity and the selectivity of these catalysts, to a great extent, differ with the specific interaction between the active metal and the support. [1, 2] Understanding the influence of the supports' structure on the metal nanoparticles has been an important issue in the areas of heterogeneous catalysis for decades. [3-5]

The methanation of CO_2, also known as Sabatier reaction, has received renewed interests,[6] not only because of environmental concern, but also due to the potential usage as chemical storage of excess H_2 generated from renewable energy. One of the major challenges for its commercial application is to develop an efficient and stable catalyst with high activity at low temperatures. Among all the investigated CO_2 methanation catalysts, Ru/TiO_2 has been regarded as the most effective one and has the highest selectivity towards CH_4.[7-9] Previous studies have demonstrated that the reduction of CO_2 requires the cooperation of Ru that is able to dissociate H_2 and the metal-support interface that is able to activate CO_2. [6b, 10] Therefore, several novel approaches have been proposed recently to obtain a highly active Ru/TiO_2 catalyst by downsizing the Ru particles, such as spray reaction method [11], polyhedral barrel sputtering technique [12], photohole-oxidation-assisted approach [13].

Although TiO_2 has been shown to be the most efficient support for Ru catalyst in CO_2 methanation reaction, [6a, 8] the effect of crystalline phases of TiO_2 on the structure and catalytic properties of Ru nano-particles has not been full recognized. Actually, in the case of Deacon reaction ($4HCl+O_2=2H_2O+2Cl_2$), the catalytic activity and stability of RuO_2 catalyst is highly dependent on the crystalline phase of TiO_2.[14] Rutile-type TiO_2 (r-TiO_2) is a much better support than anatase-TiO_2 (r-TiO_2) in stabilizing RuO_2 due to the interfacial lattice matching, resulting in a higher reactivity and stability in Deacon reaction. Therefore, we prepared the supported Ru catalysts using phase-pure r-TiO_2 and a-TiO_2, and tried to verify this effect and elucidate different catalytic performances in CO_2 methanation.

2. Experimental

2.1 Catalyst preparation

The phase-pure r-TiO_2 and a-TiO_2 supports, were synthesized as reported previously. [15] The specific area of them is 27 and 45 m^2 g^{-1}, respectively.

The Ru catalysts were prepared by a wet-impregnation method using the r-TiO_2 and a-TiO_2 supports. The weight loading of Ru was targeted at 5 wt%. Aqueous solutions (2.55 mL) of $RuCl_3$ (0.306 mol_{Ru} L^{-1} in ultra-super water, Sinopharm Chemical Reagent Co., Ltd) were diluted to 25.5 mL and heated at 50 °C stirring in water bath, then the r-TiO_2 or a-TiO_2 support (1.500 g)

[a] *State Key Laboratory of Catalysis, Dalian Institute of Chemical Physics (DICP), Chinese Academy of Sciences (CAS), Dalian 116023, China. Fax: (+) 86 411 84685940. E-mail: yqhuang@dicp.ac.cn (Y. Huang).*
[b] *State Key Laboratory of Fine Chemicals, School of Chemical engineering, Dalian University of Technology, Dalian 116024, China.*
[c] *Graduate University of Chinese Academy of Sciences, Beijing 10049, China.*
[d] *Center of Electron Microscopy and State Key Laboratory of Silicon Materials, Department of Materials Science and Engineering, Zhejiang University, Hangzhou 310027, China.*
† Electronic Supplementary Information (ESI) available: See DOI: 10.1039/b000000x/

were poured into the solution and kept stirring until the water were evaporated. And then the samples were dried at 120 °C for 12 h, and calcined in air at 300 °C for 4 h. The resultant precipitate was washed 10 more times with diluted ammonia solution and 3 times with deionizied water to remove the residual chlorides. Finally, the samples were dried at 80 °C for 8 h and reduced in H_2 at 400 °C for 1 h.

2.2 Activity test

The CO_2 methanation activities of these Ru catalysts were evaluated in a continuous-flow fixed-bed reactor operating at atmospheric pressure. The catalyst (40 mg, 20 ~ 40 mesh) diluted in 400 mg SiO_2 (20~40 mesh) was loaded in a U-shape quartz reactor (i.d. 6 mm), the feed gas containing 18 vol.% CO_2, 72 vol.% H_2 and balanced with 10 vol.% N_2 (employed as internal standard gas) was passed through the reactor at a flow rate of 50 ml min^{-1}, corresponding to a total space velocity of 75, 000 mL h^{-1} g_{cat}^{-1}.

The reactant gases and effluent gases from the reactor were first passed through an ice-bath unit to remove the water vapor, and then analyzed on line with an Agilent 6890 gas chromatograph using Helium as carrier gas. The TDX-01 column connected to a TCD detector was used to identify and quantify outlet gases (H_2, N_2, CO, CH_4 and CO_2). The CO_2 conversion was calculated based on the difference between inlet and outlet concentrations.

The CO_2 conversion was calculated by the equation as follows using the area of each detected gas:

$$\text{Conversion } (CO_2\%) = \frac{CO_2(in) - CO_2(out) * \frac{N_2(in)}{N_2(out)}}{CO_2(in)} * 100\%$$

2.3 Catalyst characterizations

X-ray diffraction (XRD) patterns were recorded with a PANalytical X'Pert-Pro powder X-ray diffractometer, using Cu Kα monochromatized radiation (λ = 0.1541 nm) at a scan speed of 5° min^{-1}.

High-angle annular dark-field scanning transmission electron microscopy (HAADF-STEM) images were obtained on a Titan G2 80-200 with ChemiSTEM. High-resolution TEM images (HRTEM) were taken on a Tecnai G2 F30 Field Emission Gun Transmission Electron Microscope.

The X-ray absorption spectra (XAS) of the Ru K-edge were measured at the BL01C1 of the National Synchrotron Radiation Research Center, Hsinchu, Taiwan. The electron storage ring is operated at 1.5 GeV with a beam current of 360 mA under a top-up injection mode. The samples were reduced in H_2 at 400 °C for 1 h, and then protected under inert atmosphere to prevent oxidation before sealing them at an oxygen-free glove box. The data analysis package (Athena, Artemis) was used for the data analysis and fitting [16].

Temperature-programmed reduction (H_2-TPR) experiments were evaluated on a Micromeritics Auto Chem II 2920 automatic catalyst characterization system. Prior to the H_2-TPR experiment, 80 mg of the sample already calcined at 300 °C for 4 h was loaded into a U-shape quartz reactor and thermally treated in air at 200 °C for 2 h to remove adsorbed carbonates and hydrates. Then, after cooling to room temperature, the flowing gas was switched to a 10 vol.% H_2-Ar, and the catalyst was heated to 900 °C at a ramping rate of 10 °C min^{-1}.

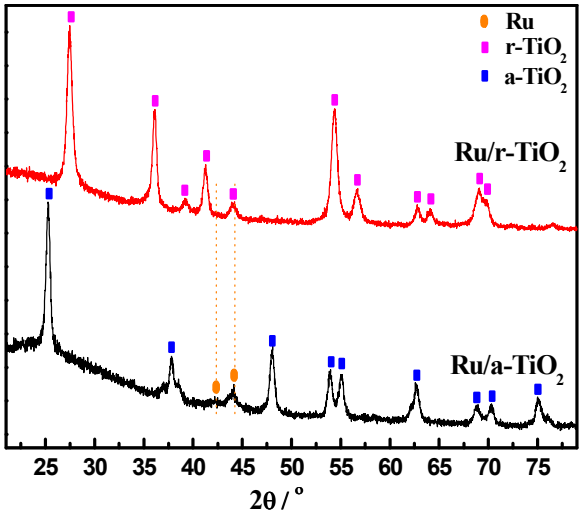

Fig. 1 The XRD patterns of supported Ru catalysts

3. Results and discussions

3.1 Distribution of the Ru catalysts over different phase type TiO_2 supports

To reveal the crystalline phase influence of the support on the structure of the Ru nanoparticles, the XRD analysis of the Ru/r-TiO_2 and Ru/a-TiO_2 catalysts were carried out as presented in Fig. 1. Except the diffraction peaks of a-TiO_2 support, the peaks at 2θ value of 42.3 ° and 44.1 °, assigned to metallic ruthenium (PDF NO. 06-0633), were observed on the Ru/a-TiO_2 catalysts. However, there were no characteristic peaks of Ru^0 observed on the rutile-type TiO_2 supported Ru/r-TiO_2 catalysts, indicating a high dispersion of Ru on the r-TiO_2 support. The representative images of the Ru/r-TiO_2 and Ru/a-TiO_2 catalysts were presented through the HAADF-STEM and HRTEM in Fig. 2, Fig. S1 and Fig. S2. From the Fig. 2a, S1a and S2a, we could easily see many severely sintered ruthenium nanoparticles larger than 10 nm on the surface of a-TiO_2 support, displaying in the shape of bright round spot or narrow strip in the HAADF-STEM images. To be noted, there were still a few Ru nanoparticles smaller than 5 nm observed from the images with high magnification (Fig. 2c). However, on the Ru/r-TiO_2, ultra-fine Ru nanopartiles with uniform particle size were dispersed on the surface of r-TiO_2 support. There were no particles larger than 3 nm observed despite of our careful observation (Fig. 2b, 2d, S1b, S2b). More intuitively, the average particle size of the Ru/a-TiO_2 catalyst was found to be 4.0 ± 2.4 nm. However, it was only 1.1 ± 0.2 nm with a quite narrower particle size distribution for the Ru/r-TiO_2 catalyst. These results indicated that the phase type of TiO_2 could remarkably affect the dispersion of Ru on its surface, and the r-TiO_2 appears to be an efficient support to stabilize nano-sized smaller particles of Ru.

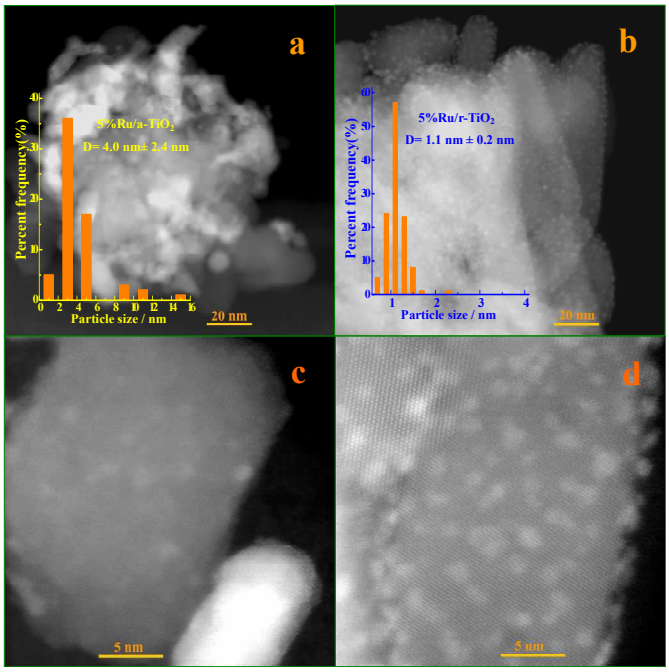

Fig. 2 HAADF-STEM images of supported Ru catalysts with high magnification

(a, c) Ru/a-TiO_2 ; **(b, d)** Ru/r-TiO_2

3.2 X-ray absorption analysis of Ru catalysts

The normalized X-ray absorption near-edge structure (XANES) spectra at the Ru K-edge of the Ru/r-TiO_2, Ru/a-TiO_2 catalysts, as well as the Ru foil, are shown in Fig. 3a. The XANES spectrum of the Ru/a-TiO_2 sample was very similar to that of the Ru foil, which indicated that the Ru species were reduced to metallic state. However, the "white line" of the Ru/r-TiO_2 sample was much higher than that of the Ru foil, which suggested that the Ru supported on rutile phase remained at oxidative state.

The nonphase-corrected, k^3-weighted extended X-ray absorption fine structure (EXAFS) spectra at the Ru K-edge for the Ru/r-TiO_2 and Ru/a-TiO_2 catalysts are shown in Fig. 3b. Consistent with the XANES results, the EXAFS spectra of Ru/a-TiO_2 sample indicates little difference from that of Ru foil. The most intense feature is Ru-Ru bond and it can be fit to the nearest

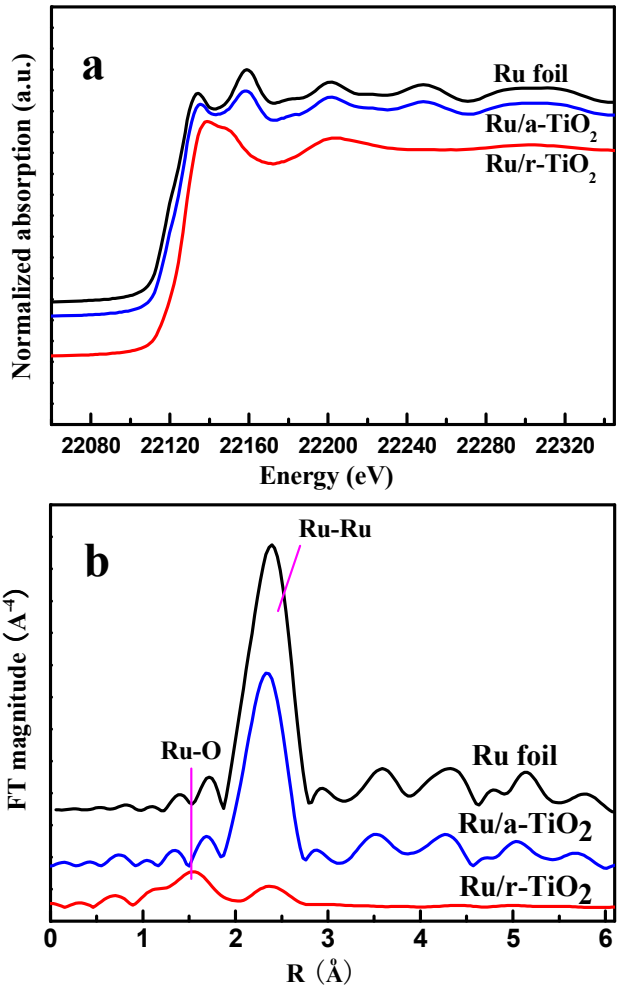

Fig. 3 (a) The normalized XANES spectra at the Ru K-edge and **(b)** Corresponding Fourier transform k^3-weighted EXAFS spectra (without phase correction) of Ru foil, Ru/r-TiO_2 and Ru/a-TiO_2.

neighbor Ru at a distance of 2.67 Å. The best fit indicates 9.8 nearest other Ru neighbors surrounding the Ru (Table 1). The theoretical particle size of Ru, obtained from the coordination numbers, [17] was about 3~4 nm, which is in good consistent with the HRTEM results. However, for the Ru/r-TiO_2 as shown in Fig. 3b, the feature of Ru-Ru bond decreased dramatically and meanwhile Ru-O bond occurred. These features described in Table 1 were fitted to only 2.2 nearest other Ru neighbors surrounding the Ru at a distance of 2.69 Å, and 4.9 nearest O neighbors at a distance of 2.00 Å also surrounding the Ru. The appearance of the Ru-O bond implies to some extent that the existence of adjacent interaction between RuO_2

Table 1 EXAFS data fitting results of of Ru foil and Ru catalysts at the Ru K-edge.

Samples	Shell	CN[a]	R(Å) [b]	$\sigma^2\times10^3$ (Å^2) [c]	ΔE_0 (eV) [d]	R-factor (%)	Δk (Å^{-1}) [e]	ΔR (Å) [f]
Ru foil	Ru-Ru	12	2.68	3.8	3.2	0.99	3.2-14.0	1.3-2.7
Ru/r-TiO_2	Ru-O	4.9	2.00	7.2	-2.8	0.40	3.0-12.1	1.2-2.8
	Ru-Ru	2.2	2.69	8.5	-2.8			
Ru/a-TiO_2	Ru-Ru	9.8	2.67	4.4	-7.1	0.89	3.2-14.0	1.5-2.7

[a] The coordination number.
[b] The average absorber-backscatterer distance.
[c] The Debye–Waller factor.
[d] The inner potential correction.
[e] The data range used for data fitting in k-space.
[f] The data range used for data fitting in R-space.

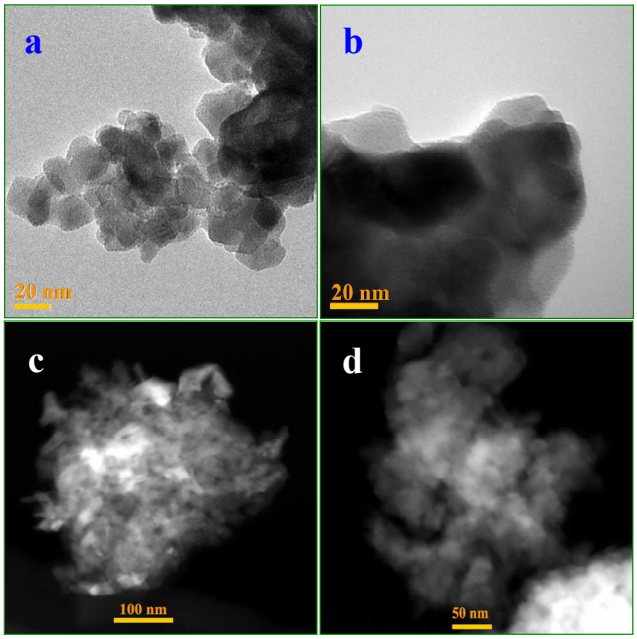

Fig. 4 (a, b) TEM images of the Ru precursor after dried at 80 ^{o}C for 12h and **(c. d)** their HAADF-STEM images after calcined in air 300 ^{o}C for 4h.

(a), $RuCl_x/a\text{-}TiO_2$; (b), $RuCl_x/r\text{-}TiO_2$;

(c), $RuO_2/a\text{-}TiO_2$; (d) $RuO_2/r\text{-}TiO_2$.

and r-TiO_2, by forming Ru-O-Ti bond as reported previously [18] which possibly stabilized the ruthenium from sintering during the process of calcination in air.

3.3 Transformation of the Ru species during the preparation process

In order to figure out how the dispersion difference happened and ascertain when the aggregation of Ru species started, we observed the Ru/a-TiO_2 and Ru/r-TiO_2 samples just dried (Fig. 4a and 4b) and those samples after calcination (Fig. 4c and 4d) by using TEM and HAADF-STEM techniques, respectively. For the just dried samples, there were no distinct Ru species observed on both of them, indicating that the Ru species were highly dispersed on both r-TiO_2 and a-TiO_2 supports and the Ru sintering did not happen at this step. The aggregation of Ru species on a-TiO_2 most likely occurred during the calcination at 300 ^{o}C. As expected, the HAADF-STEM images indicated severe aggregation of Ru species on a-TiO_2 support, and some of them were larger than 10 nm in the shape of stretched bright spot (Fig. 4c). However, RuO_2 species were still highly dispersed on the r-TiO_2 support without sintering (Fig. 4d). The possible reason is that the RuO_2, as a rutile-type oxide, had a high degree of lattice matching with r-TiO_2 (a=b=4.49 Å, c=3.11 Å for RuO_2, a=b=4.59 Å, c=2.96 Å for r-TiO_2), which led to a strong interfacial interaction by forming the Ru-O-Ti bond between RuO_2 and r-TiO_2.

To confirm this point, we characterized the calcined samples by using H_2-TPR (Fig. 5). The RuO_2 species started to be reduced at 126 ^{o}C on the a-TiO_2 support, but delayed to 160 ^{o}C on the r-TiO_2, although the RuO_2 particle size was even much smaller in the latter sample. The most likely explanation is the strong

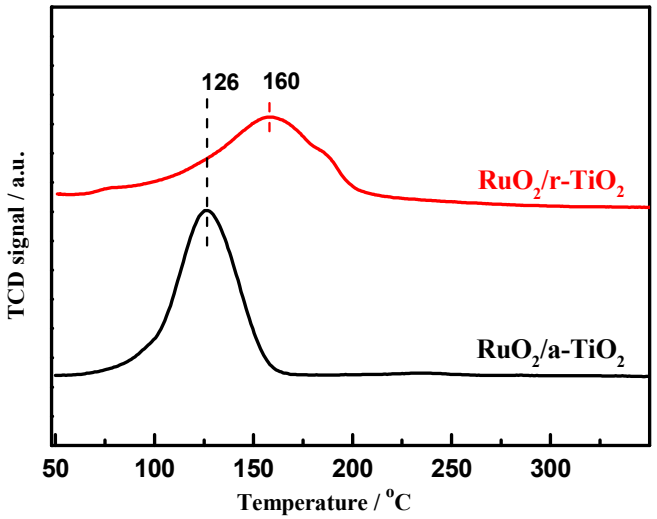

Fig. 5 The H_2-TPR profiles of the calcined RuO_2 samples (a) $RuO_2/r\text{-}TiO_2$ and (b) $RuO_2/a\text{-}TiO_2$.

interaction between RuO_2 and r-TiO_2, which hindered the reduction of RuO_2. Moreover, we also calculated the amount of H_2 consumption (Table S1) and found that there was less hydrogen consumed on the $RuO_2/r\text{-}TiO_2$ (15.4 mL_{H2} g_{cat}^{-1}) than that on the $RuO_2/a\text{-}TiO_2$ (16.8 mL_{H2} g_{cat}^{-1}). This result is consistent with the EXAFS data, indicating that the RuO_2 species were more difficult to be reduced due to the chemical bonding between RuO_2 and r-TiO_2.

It has been reported that RuO_2 nanoparticles are easily aggregated in oxidative atmosphere [19] due to the volatility of oxidized ruthenium. This is the case observed in the $RuO_2/a\text{-}TiO_2$. However, an intimate interaction occurs between RuO_2 and r-TiO_2 structure due to their high degree of lattice matching, which in turn stabilizes the RuO_2 under oxidation conditions and maintains its high dispersion.

3.4 The activities of the Ru/TiO_2 catalysts for CO_2 methanation

The CO_2 conversions as a function of reaction temperature over the Ru/r-TiO_2 and Ru/a-TiO_2 catalysts were displayed in Fig. 6a. The Ru/r-TiO_2 catalyst exhibited a much higher activity in CO_2 methanation than the Ru/a-TiO_2. At the temperature of 300 ^{o}C, about 65% CO_2 in the feed gas was converted to CH_4 on the Ru/r-TiO_2 catalysts, but the CO_2 conversion was only 34% on the Ru/a-TiO_2 catalysts. Moreover, it is worth to note that we did not detect any CO and other by-products besides CH_4, indicating that the selectivity to CH_4 on the Ru/r-TiO_2 catalysts was very high. We calculated the specific rates of the investigated catalysts at 225 ^{o}C showed in Fig. 6b. The reaction rate on the Ru/r-TiO_2 was 2.85 mol_{CO2} g_{Ru}^{-1} h^{-1}, 2.4 times higher than that on the Ru/a-TiO2 (1.19 mol_{CO2} g_{Ru}^{-1} h^{-1}), indicating that the rutile-type TiO_2 is a superior support to load Ru for CO_2 hydrogenation to CH_4. The considerable difference in CO_2 methanation activity is considered from their different particle sizes. The presence of Ru-O-Ti bond, as confirmed by EXAFS, indicated a strong interaction between Ru and r-TiO_2 support, which contributed to a higher dispersion of Ru.

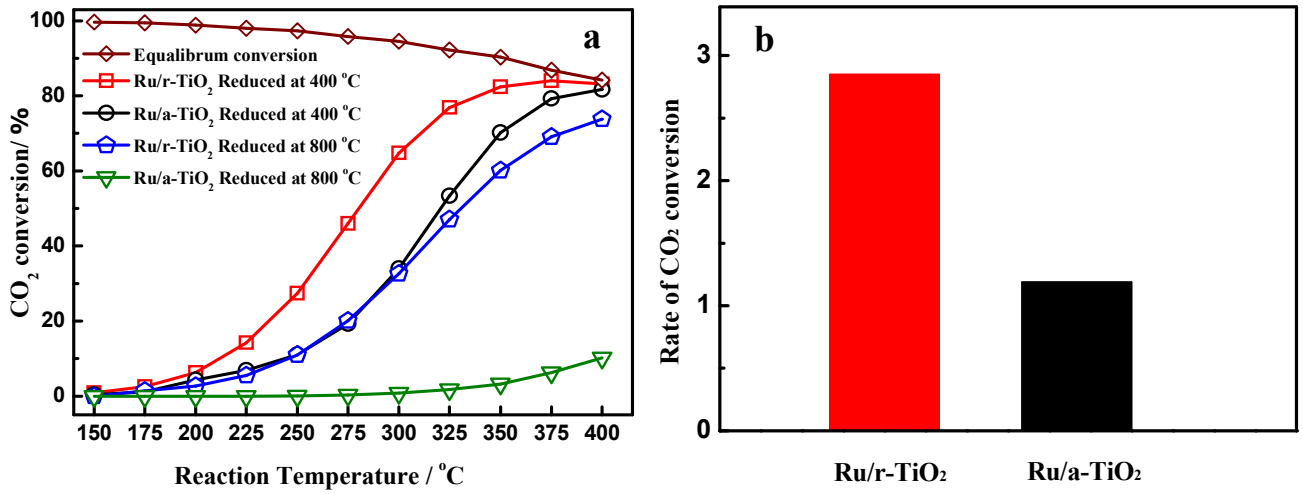

Fig. 6 **(a)** CO_2 conversions as a function of the reaction temperature for Ru catalysts and **(b)** their specific rates calculated at 225 °C.
Reaction conditions: 18 vol % CO_2 + 72 vol % H_2 + 10 vol % N_2, catalyst: Each 0.040g diluted with 0.400g SiO_2, total space velocity: 75, 000 mL g_{cat}^{-1} h^{-1}.

We also calculated the specific reaction rates of CH_4 formation related to the number of surface Ru atoms, i.e. turnover frequency (TOF) at 225 °C. An inversed correlation was obtained: the TOF over Ru/r-TiO_2 catalyst is only two thirds of that over Ru/a-TiO_2. This is consistent with previous reports that the CO_2 methanation is a structure-sensitive reaction and TOF increases with an increase of the Ru particle size [20, 21, 6b]. In addition, we have compared the specific reaction activity of our sample with that of Abe et al., one of the best results reported previously, where a complete conversion of CO_2 to CH_4 was achieved at 160 °C using a catalyst only with 0.8 wt% Ru [22]. The TOF value of our 5 wt% Ru/r-TiO_2 sample calculated at 160 °C is 6.0 × 10^{-3} s^{-1}, which is not much lower than their result (8.5 × 10^{-3} s^{-1}) as expected. The minor difference in TOF values between them can be explained by the different Ru particle size. It is 1.1 nm in our case but 3.4 nm in their case.

It is worth to note that the Ru/r-TiO_2 were very stable for CO_2 hydrogenation to CH_4 at 300 °C, without any decrease but with a slight increase, during the long-term test of over 20 h (Fig. S3). The thermal stability of these two catalysts were also compared and presented in the Fig. 6. After reduction at high temperature (800 °C), the Ru/a-TiO_2 catalyst became almost inactive in CO_2 methanation. However, there was a minor influence on the Ru/r-TiO_2 catalyst, indicating a superior thermal stability of the Ru/r-TiO_2.

All in all, the r-TiO_2 support appears to be a promising support for preparing a highly dispersed Ru catalyst, which exhibited high activity and well stability in CO_2 methanation.

4. Conclusions

The Ru dispersion was significantly influenced by the crystal phase structure of TiO_2 supports, r-TiO_2 appears to be a promising support for preparing a highly dispersed Ru catalyst with a narrow size distribution. There was a strong interaction between RuO_2 and r-TiO_2 during the calcination, which prohibited the aggregation of RuO_2. The Ru/r-TiO_2 exhibited a much higher activity and thermal stability in CO_2 methanation than the Ru/a-TiO_2. Their different catalytic performances were originated from the different particle sizes of Ruthenium. The presence of Ru-O-Ti bond hindered the aggregation of Ru nano-particles, but its contribution to the activation of CO_2 is still questioned. This work is still under progress in our group.

Notes and references

This work was supported by the NSFC (21103173, 21303194 and 51390474), 100 Talent Program of Dalian Institute of Chemical Physics (DICP). We thank Prof. Chung-Yuan Mou of National Taiwan University, Dr. Ting-Shan Chan and Dr. Jyh-Fu Lee of National Synchrotron Radiation Research Center (Hsinchu, Taiwan) for their invaluable assistance with the XAS experiments.

1 a) D. B. Clarke, I. A. T. Bell, *J. Catal.*, 1995, **154**, 314; b) A. T. Bell, *Science*, 2003, **299**, 1688.
2 a) M.S. Chen, D.W. Goodman, *Catal. Today*, 2006, **111**, 22; b) W.-J. Shen, M. Okumura, Y. Matsumura, M. Haruta, *Appl. Catal., A*, 2001, **213**, 225; c) S. Eckle, Y. Denkwitz, R.J. Behm, *J. Catal.*, 2010, **269**, 255.
3 a) S. J. Tauster, S. C. Fung, R. L. Garten, *J. Am. Chem. Soc.*, 1978, **100**, 170; b) G. L. Haller, *Adv. Catal.*, 1989, **36**, 173; c) S. E. Collins, J. J. Delgado, C. Mira, J. J. Calvino, S. Bernal, D. L. Chiavassa, M. A. Baltanás, A. L. Bonivardi, *J. Catal.*, 2012, **292**, 90; d) Q. Zhang, Y.-Z. Zuo, M.-H. Han, J.-F. Wang, Y. Jin, F. Wei, *Catal. Today*, 2010, **150**, 55.
4 a) M. S. Chen, D.W. Goodman, *Catal. Today*, 2006, **111**, 22; b) T. Akita, M. Okumura, K. Tanaka, M. Kohyama, M. Haruta, *Catal. Today*, 2006, **117**, 62.
5 a) M. Flytzani-Stephanopoulos, B. C. Gates, *Annu. Rev. Chem. Biomol. Eng.*, 2012, **3**, 545; b) M. Cargnello, V. V. T. Doan-Nguyen, T. R. Gordon, R. E. Diaz, E. A. Stach, R. J. Gorte, P. Fornasiero, C. B. Murray, *Science*, 2013, **341**, 771; c) X.-F. Yang, A. Wang, B. Qiao, J. Li, J. Liu, T. Zhang, *Acc .Chem. Res.*, 2013, **46**, 1740.
6 a) W. Wang, S. Wang, X. Ma, J. Gong, *Chem. Soc. Rev.*, 2011, **40**, 3703. b) J. H. Kwak, L. Kovarik, J. Szanyi, *ACS Catal.*, 2013, **3**, 2449; c) W. Yu, M. D. Porosoff, J. G. Chen, *Chem. Rev.*, 2012, **112**, 5780.
7 a) F. Solymosi, A. Erdöhelyi, M. Kocsis, *J. Chem. Soc., Faraday Trans.1*, 1981, **77**, 1003; b) J. A. Mieth, J. A. Schwarz, *J. Catal.*, 1989, **118**, 203.
8 Q. Jiang, G. Deng, R. Chen, Z. Huang, *Chin. J. Catal.*, 1997, **18**, 5.

9 S. Sharma, Z. Hu, P. Zhang, E. W. McFarland, H. Metiu, *J. Catal.*, 2011, **278**, 297.

10 J. H. Kwak, L. Kovarik, J. Szanyi, *ACS Catal.*, 2013, **3**, 2094.

11 M. Inoue, H. Shingen, T. Kitami,S. Akamaru, A. Taguchi, Y. Kawamoto, A. Tada, K. Ohtawa, K. Ohba, M. Matsuyama, K. Watanabe, I. Tsubone, T. Abe, *J. Phys. Chem.*, *C*, 2007, **112**, 1479.

12 D. Li, N. Ichikuni, S. Shimazu, T. Uematsu, *Appl. Catal.*, *A*, 1999, **180**, 227.

13 C. Li, S. Zhang, B. Zhang, D. Su, S. He, Y. Zhao, J. Liu, F. Wang, M. Wei, D. G. Evans, X. Duan, *J. Mater. Chem.*, *A*, 2013, **1**, 2461.

14 a) K. Seki, *Catal. Surv. Asia*, 2010, **14**, 168; b) J. Pérez-Ramírez, C. Mondelli, T. Schmidt, O. Schlüter, A. Wolf, L. Mleczko, T. Dreier, *Energ. Environ. Sci.*, 2011, **4**, 4786; c) E. V. Kondratenko, A. P. Amrute, M.-M. Pohl, N. Steinfeldt, C. Mondelli, J. Pérez-Ramírez, *Catal. Sci. Technol.*, 2013, **3**, 2555;

15 A. Sun, P. Guo, Z. Li, Y. Li, P. Cui, *J. Alloys Compd.*, 2009, **481**, 605.

16 B. Ravel, M. Newville, *J. Synchrotron Radiat.*, 2005, **12**, 537.

17 A. I. Frenkel, C. W. Hills, R. G. Nuzzo, *J. Phys. Chem. B*, 2001, **105**, 12689.

18 L. Näslund, C. M. Sánchez-Sánchez, Á. S. Ingason, J. Bäckström, E. Herrero, J. Rosen, S. Holmin, *J. Phys. Chem. C*, 2013, **117**, 6126.

19 Y. Zhang, X. Wang, Y. Zhu, T. Zhang, *Appl. Catal.*, *B*, 2013, **129**, 382.

20 a) L. Guczi, Z. Schay, K. Matusek, I. Bogyay, *Appl. Catal.*, 1986, **22**, 289; b) M. Che, *Adv. Catal.*, 1989, **36**, 55.

21 Z. Kowalczyk, K. Stołecki, W. Raróg-Pilecka, E. Miśkiewicz, E. Wilczkowska, Zbigniew Karpiński, *Appl. Catal.*, *A*, 2008, **342**, 35.

22 T. Abe, M. Tanizawa, K. Watanabe, A. Taguchi, *Energ. Environ. Sci.*, 2009, **2**, 315.